Hindawi
Wireless Communications and Mobile Computing
Volume 2022, Article ID 3262228, 10 pages
https://doi.org/10.1155/2022/3262228

Research Article

Design of the UAV Trajectory Tracking System Based on the Adaptive Neural Network - ADRC Method

Xin Cai, Xiaozhou Zhu, and Wen Yao

Defense Innovation Institute, Chinese Academy of Military Science, Beijing 100000, China

Correspondence should be addressed to Wen Yao; wendy0782@126.com

Received 1 July 2022; Accepted 31 August 2022; Published 5 October 2022

Academic Editor: Hangjun Che

In order to solve the problems of internal uncertainty and external disturbance of an unmanned aerial vehicle (UAV), this paper proposes the active disturbance rejection controller (ADRC) based on the adaptive radial basis function (RBF) neural network. Firstly, the dynamic model of a quadrotor with disturbance is analyzed and the controller is designed based on the ADRC method. Secondly, the RBF network is used to estimate the unknown parameter b of the system and the Lyapunov function is constructed to prove the stability of the closed-loop system. Finally, simulation results of a spiral ascent and a climbing maneuver flight illustrate that the controller proposed in this paper has high tracking accuracy and strong robustness under different flight scenarios; the average tracking error of the outdoor flight experiment is about 0.22 m, which further verifies the effectiveness of the proposed controller.

1. Introduction

1.1. Motivation. In recent years, quadrotors have gradually become a popular research topic. Quadrotors have many advantages, such as a simple structure, good flexibility, and vertical take-off and landing. Quadrotors not only play the important role in the military field [1, 2] but also have been widely used in the civil field [3–6]. Quadrotors have the characteristics of nonlinearity, strong coupling, and sensitivity to disturbance [7, 8]. During flight, quadrotors are generally affected by body vibration and external air flow. Moreover, a mathematical model of the UAV is difficult to accurately establish, so it is difficult to control a quadrotor UAV for position trajectory tracking.

1.2. Related Work. In controller design, it is necessary to simultaneously take into account the amount of algorithm calculation and the control effect. In the past few years, researchers worldwide have proposed many controllers for UAVs. As a classical controller, proportional integral derivative (PID) controllers have been widely used recently [9–11]. However, PID parameter tuning is difficult and it is sensitive to disturbances. In [12], a robust nonlinear controller that combines sliding mode control with backstepping control to improve the antidisturbance ability of the system was proposed. In [13], a new asymptotic tracking controller was proposed, adopting the robust integral of the signum of the error method and an immersion and invariance-based adaptive control methodology. In [14], a robust linear parameter-varying observer was designed, and then, a comparator integrator was used to design the feedback controller. In addition, there are many other methods that have been proposed, such as those involving a linear quadratic regulator [15], sliding mode control [16], and $H\infty$ control [17]. Although the above methods can achieve good anti-interference effect, they are too reliant on the system model. When the model is not accurate, the effect of the controller is greatly reduced. At the same time, many scholars use intelligent control in the design of controllers. In [18], a radial basis function neural network (RBFNN) was used to approximate the unknown system function. To simplify the model design, an adaptive network is used to approximate unknown nonlinear dynamics in [19]. In [20],

reinforcement learning was used to train a quadrotor controller to complete the hovering and trajectory tracking tasks. However, intelligent control requires a large amount of computation. The onboard CPU usually has a limited amount of computation and does not have the capability of real-time control.

Based on the advantages and disadvantages of the above methods, Han [21] proposed an active disturbance rejection controller (ADRC), which is a new type of control strategy. This controller incorporates the essence of the PID controller and solves the problem that the modern control theory is too reliant on object mathematical models. In addition, it also has the advantages of good real-time performance and strong anti-interference ability. Gao [22] linearized the design of the controller, used the bandwidth to set the parameters, and proposed a linear ADRC. At present, the ADRC has been adopted by Texas Instruments, Freescale Semiconductors, and other companies [23–25].

1.3. Contribution. ADRC still has some unsolved problems, such as compensation factor b cannot be accurately estimated, which is usually trial-and-error by manual experience method. Its stability theoretical analysis needs to be improved. At present, it has not been fully applied to the actual flight of the UAV. Aiming at the above problems, this paper designs an active disturbance rejection control system of the UAV based on the RBFNN. Our contributions are summarized as follows.

(i) The RBFNN is used to estimate the unknown compensation factor b in real time, which reduces a lot of the manual trial work

(ii) We analyze the convergence of the extended state observer (ESO) and prove the stability of the closed-loop system by constructing the Lyapunov function

(iii) We verify the effectiveness of the algorithm through simulation and further carry out a UAV anti-interference flight experiment by building a physical experimental platform

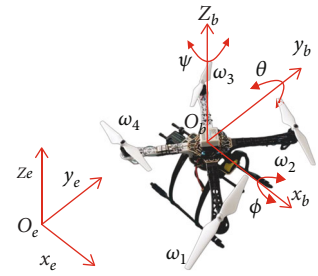

Figure 1: Structure of a quadrotor UAV with the body frame and inertial frame.

The remaining sections of this paper are organized as follows. In Section 2, the UAV dynamic model is established and the detailed problem is described. Section 3 describes the control scheme of trajectory tracking. Section 4 analyzes the convergence of ESO and proves the stability of the system. The results of simulation experiments and actual flight are provided in Section 5. Finally, the conclusion is drawn in Section 6.

2. Problem Statement

2.1. Quadrotor Dynamic Model. As shown in Figure 1, $O_b = \{x_b y_b z_b\}$ is the body fixed frame and $O_e = \{x_e y_e z_e\}$ is the inertial frame with respect to the Earth. Define $\chi = [x_e, y_e, z_e]^T$ as the UAV distance on the $x\,y\,z$ axis, $\eta = [\phi, \theta, \psi]^T$ as the roll angle, pitch angle, and yaw angle of the UAV, $V = [u, v, w]^T$ as the linear velocity vector, and $\Omega = [p, q, r]^T$ as the angular velocity vector of the quadrotor in the body frame $O_b = \{x_b y_b z_b\}$. The relationship between V and Ω is expressed as follows:

$$\begin{aligned} \dot{\chi} &= RV, \\ \dot{\eta} &= N\Omega, \end{aligned} \tag{1}$$

where

$$\begin{aligned} R &= \begin{pmatrix} \cos\psi\cos\theta & \cos\psi\sin\theta\sin\phi - \sin\psi\cos\phi & \cos\psi\sin\theta\cos\phi + \sin\psi\cos\phi \\ \sin\psi\cos\theta & \sin\psi\sin\theta\sin\phi + \cos\psi\cos\phi & \sin\psi\sin\theta\cos\phi - \cos\psi\sin\phi \\ -\sin\theta & \cos\theta\sin\phi & \cos\theta\cos\phi \end{pmatrix}, \\ N &= \begin{pmatrix} 1 & \sin\phi\tan\theta & \cos\phi\tan\theta \\ 0 & \cos\phi & -\sin\phi \\ 0 & \sin\phi/\cos\theta & \cos\phi/\cos\theta \end{pmatrix}. \end{aligned} \tag{2}$$

The UAV moves by changing the motor speed around the body, and its movement contains two parts: spatial translation motion and rotation motion. The mathematical model of the quadrotor UAV flight system can be obtained by the Euler equation and Newton's law, which can be described as follows:

$$\begin{aligned}
\ddot{x} &= \frac{1}{m}U_1(\cos\phi\sin\theta\cos\psi + \sin\phi\sin\psi) + D_1(t),\\
\ddot{y} &= \frac{1}{m}U_1(\cos\phi\sin\theta\sin\psi + \sin\phi\cos\psi) + D_2(t),\\
\ddot{z} &= \frac{1}{m}U_1(\cos\phi\cos\theta) - g + D_3(t),\\
\ddot{\phi} &= \frac{\theta\psi(I_y - I_z) + lU_2}{I_x} + D_4(t),\\
\ddot{\theta} &= \frac{\phi\psi(I_s - I_x) + U_3}{I_y} + D_5(t),\\
\ddot{\psi} &= \frac{\phi\theta(I_x - I_y) + U_4}{I_z} + D_6(t),
\end{aligned} \tag{3}$$

where I_x, I_y, I_z are the rotational inertia of the x-axis, y-axis, and z-axis, respectively, l is the length between the center of the aircraft and the rotor, and m and g are the mass of the UAV and gravitational acceleration, respectively. $D_i(i = 1, 2, 3, 4, 5, 6)$ represents the unknown total disturbances and the uncertain parts of the model. The input control $(U_1\ U_2\ U_3\ U_4)$ values are expressed as follows:

$$\begin{aligned}
U_1 &= K_F(\omega_1^2 + \omega_2^2 + \omega_3^2 + \omega_4^2),\\
U_2 &= K_F(\omega_4^2 - \omega_2^2),\\
U_3 &= K_F(\omega_3^2 - \omega_1^2),\\
U_4 &= K_M(\omega_1^2 + \omega_3^2 - \omega_2^2 - \omega_4^2),
\end{aligned} \tag{4}$$

where K_F and K_M are the lift coefficient and reverse torque coefficient, respectively, and $\omega_i(i = 1, 2, 3, 4)$ is the speed of the ith rotor.

2.2. Problem Description. The UAV dynamics equation is obtained by the above analysis. The UAV is an underactuated system with four input channels and six output channels, and there is a strong coupling relationship between its position state and attitude state. The horizontal motion of the UAV is affected by the roll angle and pitch angle at the same time.

Problem 1. The dynamic model of the UAV (3) can be rewritten as follows:

$$\begin{aligned}
\ddot{x} &= s_1(x, \dot{x}, \varpi_1) + b_1u_1,\\
\ddot{y} &= s_2(y, \dot{y}, \varpi_2) + b_2u_2,\\
\ddot{z} &= s_3(z, \dot{z}, \varpi_3) + b_3u_3,\\
\ddot{\phi} &= s_4\left(\phi, \dot{\phi}, \varpi_4\right) + b_4u_4,\\
\ddot{\theta} &= s_5\left(\theta, \dot{\theta}, \varpi_5\right) + b_5u_5,\\
\ddot{\psi} &= s_6(\psi, \dot{\psi}, \varpi_6) + b_6u_6,
\end{aligned} \tag{5}$$

where $s_i(\cdot)$ is the uncertainty of the system, $\varpi_i(\cdot)$ is the total disturbance of the system, $b_i(\cdot)$ is the compensation factor, and $u_i(\cdot)$ is the control input.

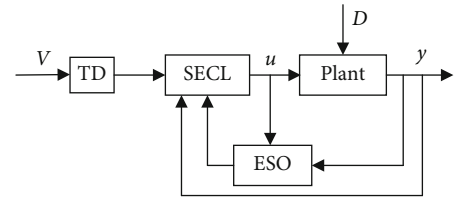

Figure 2: ADRC structure.

Let $x_1 = [x, y, z, \phi, \theta, \psi]^T$, $x_2 = [\dot{x}, \dot{y}, \dot{z}, \dot{\phi}, \dot{\theta}, \psi]^T$, $b = [b_1, b_2, b_3, b_4, b_5, b_6]^T$, $u = [u_1, u_2, u_3, u_4, u_5, u_6]^T$, and $f = [s_1, s_2, s_3, s_4, s_5, s_6]^T$. Then, (5) can be rewritten as follows:

$$\begin{aligned}
Y &= x_1,\\
\dot{x}_1 &= x_2,\\
\dot{x}_2 &= f + bu.
\end{aligned} \tag{6}$$

The key is how to estimate the total disturbance f and the compensation factor b in real time, and then, (6) becomes a cascade integrator as shown in (7), so that the design of the controller becomes simple.

$$\ddot{Y} = u_0. \tag{7}$$

2.2.1. Approach. ADRC technology has low dependence on the accuracy of the system model, can estimate and dynamically compensate the internal and external disturbances of the system, and can improve the robustness of the system. This system consists of three parts: the tracking differentiator (TD), extended state observer (ESO), and state error control law (SECL) [21]. The structure of an ADRC is shown in Figure 2. v, u, and y represent the desired signal, control input, and output signal. D is the external disturbance on the system. The roll angle ϕ is taken as an example to illustrate the specific process of the ADRC control law design, where the design of other channel controllers is similar.

3. Tracking Differentiator

A TD arranges a transition process for the attitude angle command and obtains its differential signal. Assuming that the desired roll angle is ϕ_d, the TD is expressed as follows:

$$\begin{aligned}
fh &= \text{fhan}(v_1 - \phi_d, v_2, r, h),\\
v_1 &= v_1 + hv_2,\\
v_2 &= v_2 + hfh,
\end{aligned} \tag{8}$$

where r is the speed factor and h is the filtering factor. r and h can affect the speed of signal tracking. v_1 is the tracking signal for ϕ_d and v_2 is the differential signal of v_1. The optimal synthetic rapid control function $\text{fhan}(\cdot)$ is shown as follows:

$$
\begin{aligned}
d &= rh^2,\\
a_0 &= hv_2,\\
y &= v_1 + a_0,\\
a_1 &= \sqrt{d(d+8|y|)},\\
a_2 &= \frac{a_0 + \text{sign}\,(y)(a_1 - d)}{2},\\
s_y &= \frac{[\text{sign}\,(y+d) - \text{sign}\,(y-d)]}{2},\\
a &= (a_0 + y - a_2)s_y + a_2,\\
s_a &= \frac{[\text{sign}\,(a+d) - \text{sign}\,(a-d)]}{2},\\
\text{fhan} &= -r\left[\frac{a}{d} - \text{sign}\,(a)\right]s_a - r\,\text{sign}\,(a).
\end{aligned}
\tag{9}
$$

3.1. Extended State Observer. The extended state observer is the core part of the ADRC. Its basic idea is to add the total disturbance f into system (6) as a new unknown state variable x_3, and then, system (6) can be written as follows:

$$
\begin{aligned}
Y &= x_1,\\
\dot{x}_1 &= x_2,\\
\dot{x}_2 &= x_3 + bu,\\
\dot{x}_3 &= \dot{f},
\end{aligned}
\tag{10}
$$

where x_3 is the expansion state, including the total disturbance of the system.

The extended state observer is established for the attitude channel as follows:

$$
\begin{aligned}
\dot{z}_1 &= z_2 - \beta_1\left(z_1 - y_\phi\right),\\
\dot{z}_2 &= z_3 - \beta_2\left(z_1 - y_\phi\right) + bu,\\
\dot{z}_3 &= -\beta_3\left(z_1 - y_\phi\right),
\end{aligned}
\tag{11}
$$

where $\beta_1, \beta_2, \beta_3$ are observer gains. Then, the output variables of the extended state observer (11) can track the state variables of system (10), namely, $z_1 \longrightarrow x_1$ and $z_2 \longrightarrow x_2, z_3 \longrightarrow x_3$.

3.2. RBF-Based State Error control Law. First, considering system (6), the output error of the system is as follows:

$$
e = y_d - y = y_d - x_1, \tag{12}
$$

where y_d is the command signal.

The ideal control rate is designed as follows:

$$
u^* = \frac{1}{b}\left(-x_3 + \ddot{y}_d + K^T E\right), \tag{13}
$$

where $E = [e, \dot{e}]^T$ and $K = [k_p, k_d]^T$. Make all roots of the polynomial on the left half plane of the complex plane (14) by designing K. Then, $\dot{e}(t) \longrightarrow 0, e(t) \longrightarrow 0$ when $t \longrightarrow \infty$.

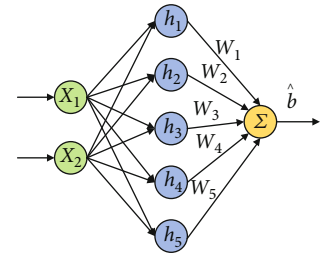

Figure 3: RBF network structure.

$$
s^2 + k_d s + k_P = 0. \tag{14}
$$

In this paper, the total disturbance x_3 is estimated based on z_3 and b is estimated by the RBFNN.

The RBFNN has the advantages of a strong generalization ability and simple network structure and can approximate any nonlinear function. Therefore, the RBFNN is used to estimate the unknown variable b of the system.

As shown in Figure 3. The designed RBFNN is a three-layer neural network composed of two input parameters, five hidden layer neurons, and one output parameter. The expression of the network output is as follows:

$$
\hat{b}(x) = \hat{W}^T h(x), \tag{15}
$$

where $x = [e, \dot{e}]^T$ is the input vector, $\hat{W}$ is the weight vector, and h is the excitation function of the hidden layer:

$$
h_j = \exp\left(-\frac{x - c_j^2}{2b_j^2}\right) j = 1, 2, 3, 4, 5, \tag{16}
$$

where c is the center of the basis function and b is the width of the Gaussian function.

Finally, the control law can be rewritten as follows:

$$
u = \frac{1}{\hat{b}(x)}\left(-z_3 + \ddot{y}_d + K^T E\right). \tag{17}
$$

4. System Stability Analysis

The mathematical model of UAVs consists of three position channels and three attitude channels. Each channel can be written as the same state equation; then, (10) is rewritten as follows:

$$
\begin{aligned}
\dot{x} &= Ax + Bu + F\dot{f},\\
y &= Cx,
\end{aligned}
\tag{18}
$$

where

$$x = \begin{bmatrix} y \\ \dot{y} \\ f \end{bmatrix},$$
$$A = \begin{bmatrix} 0 & 1 & 0 \\ 0 & 0 & 1 \\ 0 & 0 & 0 \end{bmatrix},$$
$$B = \begin{bmatrix} 0 \\ b \\ 0 \end{bmatrix}, \tag{19}$$
$$C = [1 \quad 0 \quad 0],$$
$$F = \begin{bmatrix} 0 \\ 0 \\ 1 \end{bmatrix}.$$

The extended state observer of (18) can be constructed as follows:

$$\begin{aligned} \dot{z} &= Az + Bu + L(y - \hat{y}), \\ \hat{y} &= Cz, \end{aligned} \tag{20}$$

where $L = [\beta_1 \ \ \beta_2 \ \ \beta_3]^{\mathrm{T}}$ are observer gain parameters.

4.1. Convergence Analysis of ESO. First, combining (18) and (20), the error equation is constructed and can be written as follows:

$$\begin{aligned} \dot{E}_1 &= -\beta_1 E_1 + E_2, \\ \dot{E}_2 &= -\beta_2 E_1 + E_3, \\ \dot{E}_3 &= -\beta_3 E_1 + \dot{f}, \end{aligned} \tag{21}$$

where $E_i(t) = x_i(t) - z_i(t), i = 1, 2, 3$; let $\zeta_i(t) = E_i(t)/\omega_0^{i-1}, i = 1, 2, 3$ and (21) can be rewritten as follows:

$$\begin{aligned} \zeta_1(t) &= -\frac{\beta_1}{\omega_0^0}\zeta_1 + \omega_0\zeta_2, \\ \zeta_2(t) &= -\frac{\beta_2}{\omega_0^1}\zeta_1 + \omega_0\zeta_3, \\ \zeta_3(t) &= -\frac{\beta_3}{\omega_o^2}\zeta_1 + \frac{j}{\omega_0^2}. \end{aligned} \tag{22}$$

Then, (21) can be written as the following state equation:

$$\dot{E} = (A - LC)E + F\dot{f} \triangleq \bar{\mathrm{A}}E + F\dot{f}, \tag{23}$$

where

$$\bar{\mathrm{A}} \triangleq A - LC = \begin{bmatrix} -\beta_1 & 1 & 0 \\ -\beta_2 & 0 & 1 \\ -\beta_3 & 0 & 0 \end{bmatrix}. \tag{24}$$

According to the bandwidth parameterization method proposed in [22], if the ESO eigenvalues are all configured at $-\omega_0$ (observer bandwidth) of the left half plane of S, then, $\bar{\mathrm{A}}$ is the Hurwitz matrix and the Hurwitz characteristic equation of the error system is as follows:

$$L(s) = |sI - \bar{\mathrm{A}}| = (s + \omega_0)^3. \tag{25}$$

Solving (25), the observer gain matrix L can be obtained:

$$L = \begin{bmatrix} 3\omega_o & 3\omega_o^2 & \omega_o^3 \end{bmatrix}. \tag{26}$$

Then (22) can be expressed as follows:

$$\dot{\zeta}(t) = \omega_o \mathrm{H}\zeta(t) + \Pi\frac{\dot{f}}{\omega_o^2}, \tag{27}$$

where

$$H = \begin{bmatrix} -3 & 1 & 0 \\ -3 & 0 & 1 \\ -3 & 0 & 0 \end{bmatrix},$$
$$\Pi = \begin{bmatrix} 0 \\ 0 \\ 1 \end{bmatrix}. \tag{28}$$

Lemma 1. *Assuming that $\dot{f}$ is bounded, then, there exist a positive constant $\kappa_i > 0$ and a finite time $T > 0$, such that $|E_i(t)| \le \kappa_i, i = 1, 2, 3, \forall t \ge T > 0$.*

Proof. Solving (27), the following result can be obtained:

$$\zeta(t) = e^{\omega_o H t}\zeta(0) + \int_0^t e^{\omega_o H(t-\tau)}\Pi\frac{\dot{f}}{\omega_o^2}d\tau. \tag{29}$$

Let

$$\Gamma(t) = \int_0^t e^{\omega_o H(t-\tau)}\prod\frac{f}{\omega_o^2}d\tau. \tag{30}$$

According to $|f| \le d(d > 0)$, then,

$$|\Gamma_i(t)| \le \frac{d}{\omega_o^3}\left[\left|\left(H^{-1}\Pi\right)_i\right| + \left|\left(H^{-1}e^{\omega_o H t}\Pi\right)_i\right|\right]. \tag{31}$$

Since

$$H^{-1} = \begin{bmatrix} 0 & 0 & -1 \\ 1 & 0 & -3 \\ 0 & 1 & -3 \end{bmatrix}, \tag{32}$$

then

$$\left|\left(H^{-1}\Pi\right)_i\right| = \begin{cases} 1, & i = 1, \\ 3, & i = 2, 3. \end{cases} \tag{33}$$

Since H is a Hurwitz matrix, there exists a finite time $T > 0$ for all $t \geq T, i, j = 1, 2, 3$ such that

$$\begin{aligned} \left|\left(e^{\omega,m}\right)_{ij}\right| &\leq \frac{1}{\omega_o^3}, \\ \left|\left(e^{\omega,Ht}\Pi\right),\right| &\leq \frac{1}{\omega_o^3}. \end{aligned} \tag{34}$$

Since T depends on $\omega_o A$ [26], then, set

$$\begin{aligned} A^{-1} &= \begin{bmatrix} m_{11} & m_{12} & m_{13} \\ m_{21} & m_{22} & m_{23} \\ m_{31} & m_{32} & m_{33} \end{bmatrix}, \\ e^{\omega,At} &= \begin{bmatrix} n_{11} & n_{12} & n_{13} \\ n_{21} & n_{22} & n_{23} \\ n_{31} & n_{32} & n_{33} \end{bmatrix}, \end{aligned} \tag{35}$$

for all $t \geq T$,

$$\left|\left(A^{-1}e^{u,At}B\right)_i\right| = \left|m_{i1}n_{13} + m_{i2}n_{23} + m_{i3}n_{33}\right| \leq \begin{cases} \frac{1}{\omega_0^3}, & i = 1, \\ \frac{4}{\omega_0^3}, & i = 2, 3. \end{cases} \tag{36}$$

Combining (31), (33), and (36), then,

$$|\Gamma_i(t)| \leq \frac{3d}{\omega_o^3} + \frac{4d}{\omega_o^6}. \tag{37}$$

Let $\zeta_{\max}(0) = |\zeta_1(0)| + |\zeta_2(0)| + |\zeta_3(0)|$, for all $t \geq T\, i = 1, 2, 3$.

$$\left|\left[e^{\omega,At}\zeta(0)\right]_i\right| \leq \frac{\zeta_{\max}(0)}{\omega_0^3}. \tag{38}$$

Then,

$$|\zeta_i(t)| \leq \frac{\zeta_{\max}(0)}{\omega_0^3} + \frac{3d}{\omega_0^3} + \frac{4d}{\omega_0^6}. \tag{39}$$

Let $E_{\max}(0) = |E_1(0)| + |E_2(0)| + |E_3(0)|$, according to $\zeta_i(t) = E_i(t)/\omega_o^{i-1}$ and (37), (38), and (39). Then,

$$|E_i(t)| \leq \frac{E_{\max}(0)}{\omega_{\mathrm{o}}^3} + \frac{3d}{\omega_{\mathrm{o}}^{4-i}} + \frac{4d}{\omega_{\mathrm{o}}^{7-i}} = \kappa_i. \tag{40}$$

According to (40), if $d > 0$ is a positive constant, then, the estimation errors of the ESO are convergent, and when adjusting the bandwidth ω_o of the observer, $|E_i(t)| \longrightarrow 0$. □

4.2. System Stability Analysis. The adaptive law of the weight value in the RBFNN is designed as follows:

$$\dot{\hat{\mathbf{W}}} = -\gamma E^T P \Theta h(x) \frac{1}{\widehat{b}(x)}\left(-z_3 + \ddot{y}_d + K^T E\right), \tag{41}$$

where γ is a positive constant and P is a positive definite matrix and satisfies the Lyapunov equation.

Combining (6) and (17),

$$\ddot{e} = -K^T E + (z_3 - x_3) + \left(\widehat{b}(x) - b\right)u. \tag{42}$$

According to Lemma 1, by adjusting the bandwidth ω_0 of the observer, $(z_3 - x_3) \longrightarrow 0$, (42) can be simplified as follows:

$$\ddot{e} = -K^{\mathrm{T}} E + \left(\widehat{b}(x) - b\right)u. \tag{43}$$

Let

$$\begin{aligned} \Lambda &= \begin{bmatrix} 0 & 1 \\ -k_p & -k_d \end{bmatrix}, \\ \Theta &= \begin{bmatrix} 0 \\ 1 \end{bmatrix}. \end{aligned} \tag{44}$$

Equation (43) can be expressed as follows:

$$\dot{E} = \Lambda E + \Theta\left(\widehat{b}(x) - b\right)u. \tag{45}$$

The optimal parameter is defined as follows:

$$W^* = \arg \min_{W \in \Omega}\left[\sup\left|\widehat{b}(x) - b\right|\right], \tag{46}$$

where Ω is a set of W.

The neural network approximation error is defined as follows:

$$\varepsilon = \widehat{b}(x|W^*) - b(x). \tag{47}$$

Equation (45) can be written as follows:

$$\dot{E} = \Lambda E + \Theta\left(\left(\widehat{W} - W^*\right)^T h(x) + \varepsilon\right)u. \tag{48}$$

Table 1: The parameter values of the quadrotor UAV.

Parameter	Value	Parameter	Value
$m/(\mathrm{kg})$	1.2	$I_x(\mathrm{kg/m^2})$	0.033
$g/(\mathrm{m/s^2})$	9.8	$I_y(\mathrm{kg/m^2})$	0.033
$l/(\mathrm{m})$	0.28	$I_z(\mathrm{kg/m^2})$	0.048

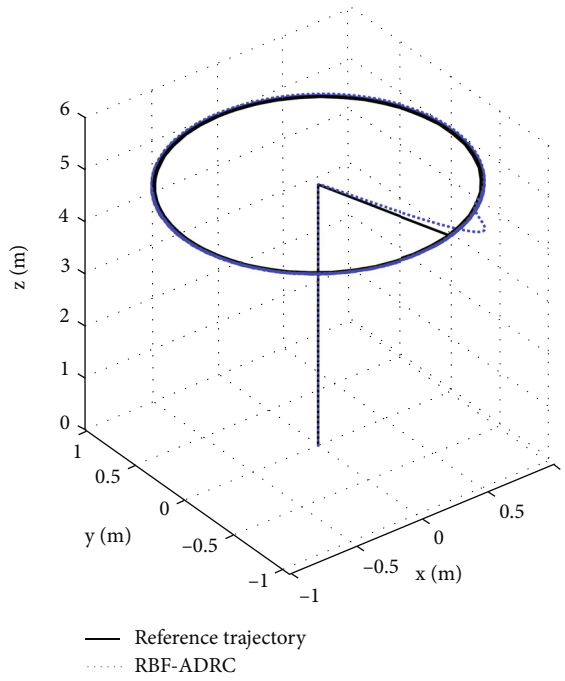

Figure 4: Three-dimensional dynamical tracking results.

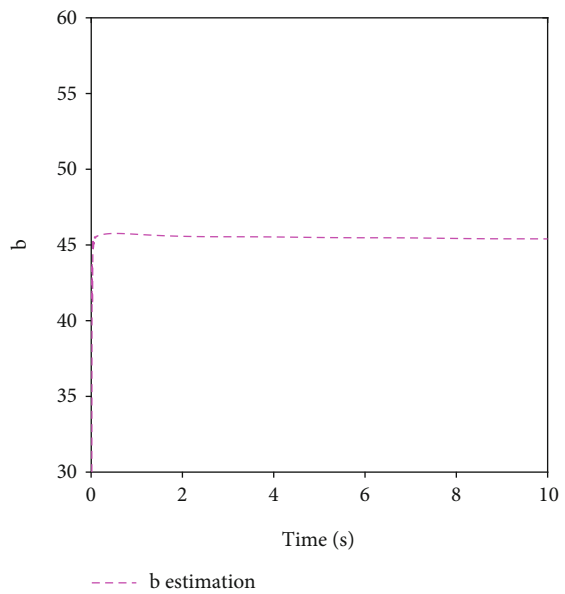

Figure 5: System parameter curve approximated by RBF.

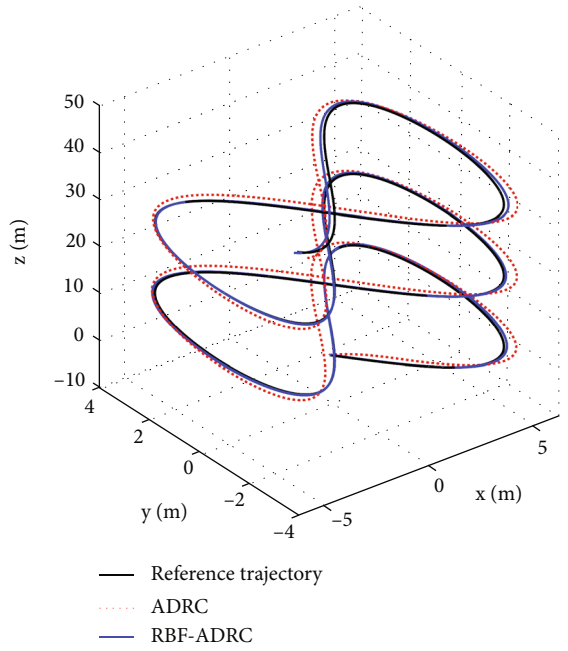

Figure 6: Trajectory tracking control response.

The Lyapunov function is defined as follows:

$$V = \frac{1}{2}E^T PE + \frac{1}{2\gamma}\left(\widehat{W} - W^*\right)^T\left(\widehat{W} - W^*\right), \tag{49}$$

where P satisfies the Lyapunov equation:

$$\Lambda^T P + P\Lambda = -Q. \tag{50}$$

Define $M = B((\widehat{W} - W^*)^T h(x) + \varepsilon)u$, $V_1 = 1/2E^T PE$, and $V_2 = (1/2\gamma)(\widehat{W} - W^*)^T(\widehat{W} - W^*)$; then, the time derivative of V_1 is as follows:

$$\begin{aligned}\dot{V}_1 &= \frac{1}{2}\dot{E}^T PE + \frac{1}{2}E^T P\dot{E}\\ &= \frac{1}{2}\left(E^T\Lambda^T + M^T\right)PE + \frac{1}{2}E^T P(AE + M)\\ &= \frac{1}{2}E^T\left(\Lambda^T P + PA\right)E + \frac{1}{2}M^T PE + \frac{1}{2}E^T PM\\ &= -\frac{1}{2}E^T QE + \frac{1}{2}\left(M^T PE + E^T PM\right)\\ &= -\frac{1}{2}E^T QE + E^T PM.\end{aligned} \tag{51}$$

Substituting M into (51) gets as follows:

$$\begin{aligned}\dot{V}_1 &= -\frac{1}{2}E^T QE + E^T P\Theta\left(\widehat{W} - W^*\right)^T h(x)u + E^T P\Theta\varepsilon u\\ &= -\frac{1}{2}E^T QE + \left(\widehat{\mathrm{W}} - \mathrm{W}^*\right)^T EP\Theta h(x)u + E^T P\Theta\varepsilon u.\end{aligned} \tag{52}$$

The derivative of V_2 is as follows:

$$\dot{V}_2 = \frac{1}{\gamma}\left(\widehat{W} - W^*\right)^T \dot{\widehat{W}}. \tag{53}$$

Therefore, the derivative of the Lyapunov function V is obtained as follows:

$$\begin{aligned}\dot{V} = \dot{V}_1 + \dot{V}_2 = -\frac{1}{2}E^T QE + E^T P\Theta\varepsilon u \\ + \frac{1}{\gamma}\left(\widehat{W} - W^*\right)^T \left(\dot{\widehat{W}} + \gamma E^T P\Theta h(x)u\right).\end{aligned} \tag{54}$$

Substituting the adaptive law (41) into the above equation can be obtained as follows:

$$\begin{aligned}\dot{V} &= -\frac{1}{2}E^T QE + E^T P\Theta\varepsilon u \\ &= -\frac{1}{2}E^T QE + \frac{\varepsilon E^T P\Theta}{\widehat{b}_0(x)}\left(-z_3 + \ddot{y}_d + K^T E\right).\end{aligned} \tag{55}$$

Due to $-1/2E^T QE \le 0$, the RBFNN can be designed to make the error $\varepsilon \longrightarrow 0$, such that $\dot{V} \le 0$.

5. Experiment Results

5.1. Simulation Result. In this section, the proposed controller is simulated and compared with the classical ADRC controller for scenarios involving external disturbance and model uncertainty (internal disturbance) to verify the effectiveness of the control scheme. Set the initial position coordinates of the quadrotor as $[0, 0, 0]$ while the initial attitude is $[0, 0, 0]$. The parameters of the quadrotor model are shown in Table 1.

Case 1. In this case, the rounded desired trajectory is set as follows. When $0 < t < 5s, x_d = 0; y_d = 0; z_d = t; \psi_d = 0$, and when $t > 5, x_d = \cos(2t); y_d = \sin(2t); z_d = 5; \psi_d = 0$. The tracking result of the quadrotor is shown in Figure 4. The estimated curve of the system unknown parameter b by the RBF neural is shown in Figure 5. It can be seen that the estimated value of the neural network converges to a small bounded range in a very short period of time. This method saves a lot of time than manual adjustment of parameters.

Case 2. In this case, set the desired climbing trajectory as follows: $x_d = 6 \times \sin(t/3); y_d = -6 \times \sin(t/3)\cos(t/3); z_d = 0.8t$; to verify the resistance of the UAV to external disturbance, during the flight of the quadrotor UAV, white noise with a peak value of 6 is added to the UAV as an external disturbance. Figure 6 shows the trajectory tracking results; in this figure, it is clear that the RBF-ADRC can well overcome external disturbances and track the desired trajectory. Moreover, the ADRC controller is affected by external disturbances and there are many oscillations that deviate from the reference trajectory.

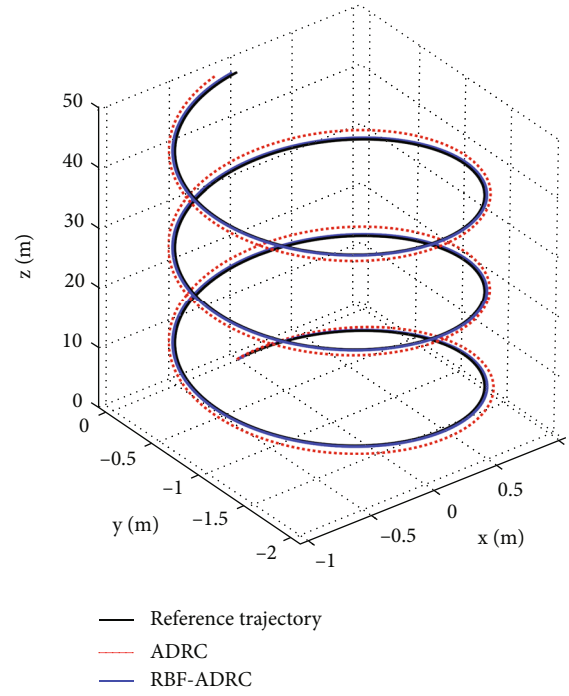

Figure 7: Trajectory tracking control (parameter-changed) response.

Case 3. To further verify the ability of the UAV to overcome model uncertainty (internal uncertainty), a spiral curve is used as the reference trajectory. The cylindrical spiral can be defined as follows: $x_d = \cos(0.1\pi t); y_d = \cos(0.1\pi t) - 1; z_d = 0.8t$. The parameters of the ADRC controller and RBF-ADRC remain unchanged, and the UAV model parameters in Table 1 are reduced by 30%. The tracking result of the UAV is shown in Figure 7, demonstrating that the RBF-ADRC controller can still ensure good trajectory tracking accuracy. Moreover, the ADRC controller is clearly affected by the change in model parameters and the tracking error becomes larger. The simulation results show that when the UAV model parameters change, the RBF-ADRC also has good robustness and high tracking accuracy.

5.2. Actual Flight Experiment. The self-built quadrotor UAV integrates the BMI088IMU module and HC-SR04 ultrasonic module. The actuator unit selects 9450 self-tightening propellers, Xrotor-30A electronic speed controllers, and sunnyskyKV-980dc motors. The UAV transmits data to the monitoring computer for display and recording through the 2.4 GHz wireless module. The designed controller code is embedded in the Raspberry Pi. The attitude control frequency is 200 Hz and the position loop frequency is 50 Hz. The effectiveness of the algorithm is verified by the fixed-point (0,0) flight of the UAV.

In order to simulate the state of the quadrotor UAV under unknown disturbance, A 550 ml bottle containing 300 ml water is attached to the arm of the UAV (as shown in Figure 8). The rope tied to the bottle will swing and the water in the bottle will shake. At the same time, considering the influence of the wind in the outdoor environment, the quadrotor UAV is finally strongly disturbed and the disturbance is

Figure 8: Flight test under strong disturbance.

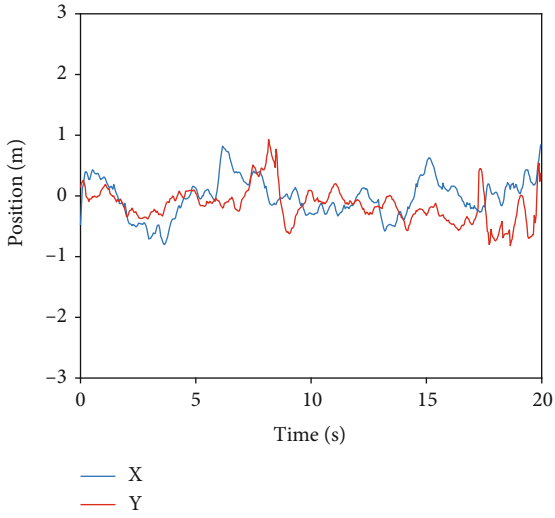

Figure 9: Actual flight results.

highly uncertain. During flight, from the coordinate values in the x and y directions of the actual flight of the UAV in Figure 9, it can be seen that the UAV can still be positioned near the origin (0,0) and the position swing amplitude is small. The average value of tracking error is about 0.22 m. The test results show that the quadrotor UAV can still maintain its stability under the influence of external interference with variable amplitude, frequency, and direction.

6. Conclusion

This paper proposes the method that combines ADRC and the neural network to solve the problem of stable flight of the UAV under multiple disturbances. The method uses the RBF neural network to estimate the unknown parameters of the system, and it can converge to a smaller range in a short time. Finally, not only the effectiveness of the method in various scenarios is shown by numerical simulations but also the robustness of the algorithm is further verified by real flight experiments in complex outdoor environments. This paper provides an effective link between the control theory and practical applications. In the future, we will extend the research to the multi-UAV cooperative control system. In the flight process, there exist problems such as air flow disturbance and load swing among multiple UAVs, which brings great challenges to the design of the multi-UAV System. Therefore, the method proposed in this paper will be helpful to solve the problem.

Data Availability

The data used to support the findings of this study are available from the corresponding author upon request.

Conflicts of Interest

The authors declare that they have no conflicts of interest.

Acknowledgments

The research is supported by the National Natural Science Foundation of China under Grant 11725211.

References

[1] S. L. de Oliveira, B. R. A. de Mello, and V. B. G. Campos, "Proposal to planning facility location using UAV and geographic information systems in a post-disaster scenario," *International Journal of Disaster Risk Reduction*, vol. 36, p. 101080, 2019.

[2] T. Yang, S. Wang, and J. Yang, "Design of high-power dual-redundancy electro-mechanical actuator for scout and strike UAV," in *IOP Conference Series: Materials Science and Engineering*, vol. 790, Bangkok, Thailand, 2020no. 1.

[3] H. Menouar, I. Guvenc, K. Akkaya, A. S. Uluagac, A. Kadri, and A. Tuncer, "UAV-enabled intelligent transportation systems for the smart city: applications and challenges," *IEEE Communications Magazine*, vol. 55, no. 3, pp. 22–28, 2017.

[4] X. Zhang and L. Duan, "Fast deployment of UAV networks for optimal wireless coverage," *IEEE Transactions on Mobile Computing*, vol. 18, no. 3, pp. 588–601, 2019.

[5] Z. Wang and L. Duan, "Chase or wait: dynamic UAV deployment to learn and catch time-varying user activities," *In IEEE Transactions on Mobile Computing*, p. 1, 2021.

[6] X. Wang and L. Duan, "Economic analysis of unmanned aerial vehicle (UAV) provided mobile services," *IEEE Transactions on Mobile Computing*, vol. 20, no. 5, pp. 1804–1816, 2021.

[7] Y. Zou and B. Zhu, "Adaptive trajectory tracking controller for quadrotor systems subject to parametric uncertainties," *Journal of the Franklin Institute*, vol. 354, no. 15, pp. 6724–6746, 2017.

[8] D. J. Zhao and D. G. Yang, "Model-free control of quadrotor vehicle via finite-time convergent extended state observer," *International Journal of Control, Automation and Systems*, vol. 14, no. 1, pp. 242–254, 2016.

[9] R. R. Benrezki, M. Tadjine, F. Yacef, and O. Kermia, "Passive fault tolerant control of quadrotor UAV using a nonlinear PID," in *2015 IEEE International Conference on Robotics and Biomimetics (ROBIO)*, pp. 1285–1290, Zhuhai, China, December 2015.

[10] F. Goodarzi, D. Lee, and T. Lee, "Geometric nonlinear PID control of a quadrotor UAV on SE (3)," in *2013 European control conference (ECC)*, pp. 3845–3850, Zurich, Switzerland, July 2013.

[11] W. Si, H. She, and Z. Wang, "Fuzzy PID controller for UAV tracking moving target," in *2017 29th Chinese Control And*

Decision Conference (CCDC), pp. 3023–3027, Chongqing, China, May 2017.

[12] F. Chen, R. Jiang, K. Zhang, B. Jiang, and G. Tao, "Robust backstepping sliding-mode control and observer-based fault estimation for a quadrotor UAV," *IEEE Transactions on Industrial Electronics*, vol. 63, no. 8, pp. 5044–5056, 2016.

[13] B. Zhao, B. Xian, Y. Zhang, and X. Zhang, "Nonlinear robust adaptive tracking control of a quadrotor UAV via immersion and invariance methodology," *IEEE Transactions on Industrial Electronics*, vol. 62, no. 5, pp. 2891–2902, 2015.

[14] F. R. López-Estrada, J. C. Ponsart, D. Theilliol, Y. Zhang, and C. M. Astorga-Zaragoza, "LPV model-based tracking control and robust sensor fault diagnosis for a quadrotor UAV," *Journal of Intelligent & Robotic Systems*, vol. 84, no. 1-4, pp. 163–177, 2016.

[15] M. Farrell, J. Jackson, J. Nielsen, C. Bidstrup, and T. McLain, "Error-state LQR control of a multirotor UAV," in *2019 International Conference on Unmanned Aircraft Systems (ICUAS)*, pp. 704–711, Atlanta, GA, USA, June 2019.

[16] M. Labbadi and M. Cherkaoui, "Robust integral terminal sliding mode control for quadrotor UAV with external disturbances," *International Journal of Aerospace Engineering*, vol. 2019, Article ID 2016416, 10 pages, 2019.

[17] J. López, R. Dormido, S. Dormido, and J. P. Gómez, "A robust H∞ controller for an UAV flight control system," *The Scientific World Journal*, vol. 2015, Article ID 403236, 11 pages, 2015.

[18] M. Chen, G. Tao, and B. Jiang, "Dynamic surface control using neural networks for a class of uncertain nonlinear systems with input saturation," *IEEE Transactions on Neural Networks and Learning Systems*, vol. 26, no. 9, pp. 2086–2097, 2015.

[19] O. Doukhi and D. J. Lee, "Neural network-based robust adaptive certainty equivalent controller for quadrotor UAV with unknown disturbances," *International Journal of Control, Automation and Systems*, vol. 17, no. 9, pp. 2365–2374, 2019.

[20] C. H. Pi, K. C. Hu, S. Cheng, and I. C. Wu, "Low-level autonomous control and tracking of quadrotor using reinforcement learning," *Control Engineering Practice*, vol. 95, p. 104222, 2020.

[21] J. Han, "From PID to active disturbance rejection control," *IEEE Transactions on Industrial Electronics*, vol. 56, no. 3, pp. 900–906, 2009.

[22] Z. Gao, "Scaling and bandwidth-parameterization based controller tuning," in *Proceedings of the American control conference*, vol. 6, pp. 4989–4996, Denver, Colorado, USA, 2003.

[23] Z. Wu, D. Li, and Y. Q. Chen, "Active disturbance rejection control design based on probabilistic robustness for uncertain systems," *Industrial & Engineering Chemistry Research*, vol. 59, no. 40, pp. 18070–18087, 2020.

[24] Z. Wang, J. Li, and D. Duan, "Manipulation strategy of tilt quad rotor based on active disturbance rejection control," *Proceedings of the Institution of Mechanical Engineers, Part G: Journal of Aerospace Engineering*, vol. 234, no. 3, pp. 573–584, 2020.

[25] S. Shen and J. Xu, "Attitude active disturbance rejection control of the quadrotor and its parameter tuning," *International Journal of Aerospace Engineering*, vol. 2020, Article ID 8876177, 15 pages, 2020.

[26] Q. Zheng, L. Dong, D. H. Lee, and Z. Gao, "Active disturbance rejection control for MEMS gyroscopes," in *2008 American control conference*, vol. 2008, pp. 4425–4430, Seattle, WA, USA, June 2008.